Electronic Supplementary Information

Trade-off between Carbohydrates and Metal Ions Regulates Chemotactic Directionality of Alkaline Phosphatase

Akshi Deshwal, Shikha, Subhabrata Maiti*

Department of Chemical Sciences, Indian Institute of Science Education and Research (IISER) Mohali, Knowledge City, Manauli 140306, India.

E-mail: smaiti@iisermohali.ac.in

Table of Contents

1. Experimental Section:

1.1 Materials and methods:

All commercially available reagents were used without further any purification. Alkaline Phosphatase (ALP) from *Bovine Calf Intestine* (P7640) and p- nitrophenyl phosphate (PNPP) were procured from Sigma Guanidium Hydrochloride (GDNHCl), Fluorescein isothiocyanate (FITC) and HEPES buffer, carbohydrates (Fructose, Glucose and Sucrose), Zinc nitrate ($ZnNO_3$) and Calcium Nitrate ($Ca(NO_3)_2$) and Sodium Nitrate ($NaNO_3$) were purchased from Sisco Research Laboratory (SRL) Magnesium nitrate ($Mg(NO_3)_2$) were purchased from Molychem.

UV-Vis studies were performed using Varian Cary 60 (Agilent technologies) spectrophotometer. The total volume was fixed at 1 ml and cuvette of path length 1 cm was used for the entire kinetic study. All measurements have been performed at 25 ^oC. Fluorescence measurements were performed using Cary Eclipse Fluorescence Spectro- fluorometer.

The optical and fluorescence microscopic images were collected using Zeiss Axis Observer 7 microscope having AxioCam 503 Mono 3 Mega pixel with ZEN 2 software.

The Dynamic Light Scattering (DLS) data was recorded on Horiba Scientific Nanoparticle Analyzer SZ-100V2. In order to measure the size, zeta potential and diffusion coefficient, for the entire study 5 µM ALP, 100 mM sugars and 1 mM ions were used. For each sample six repeated measurements after every 30 sec were performed at room temperature 25^oC.

Circular Dichroism (CD) Measurements were performed using Chirascan Spectrophotometer (Applied Photophysics) using a 1 mm path length quartz cell. The concentration of Alkaline phosphatase, Sugars and Ions used for the CD measurement were 2 µM, 100mM, 1mM respectively. The spectra were recorded over a scan range of 200-280 nm. For each sample three repeated measurements were recorded.

Viscosity measurements of different sugars solutions were carried out using Ostwald viscometer and their densities were measured by density bottle method. All of the viscosity's values were calculated using the formula given below, where water was considered as a standard liquid having a density of 1 g/ml at 25^0C.

$$\eta_1 = ƒ_1t_1/ƒ_2t_2 \times \eta_2$$

where $ƒ_1$: density of sugar solutions $\qquad$ η_1: viscosity of unknown solution i.e., sugar

t_1: time flow of sugar solutions $\qquad$ $ƒ_2$: density of standard liquid i.e., water

t_2: time flow of water

1.2 Preparation of FITC Tagged Alkaline phosphatase:

FITC tagged alkaline phosphatase was prepared as given in literature [S1]. 1 mg/ml FITC was dissolved in DMSO and then 100 µl of this was mixed with 8 mg/ml of alkaline phosphatase. The solution was kept under dark at 4 °C for 5 to 6 hrs. After that the ongoing reaction of tagging was quenched by addition of 50 mM of ammonium chloride and the mixture was kept for more 2 hrs. Then the reaction mixture was passed through a column made up of Sephadex G-25 and the formed conjugate was purified through column with 10 mM HEPES buffer (pH= 7). The eluted samples were collected in the different vials and their UV absorption spectra were recorded in which FITC-ALP conjugate showed absorption maxima at 280nm peak and FITC at 495nm. Tagging efficiency of ALP was found 0.6, means a single enzyme has an average of 0.6 FITC molecule.

1.3 Tertiary structure studies

Tertiary structure studies were performed using a quartz cuvette with a fixed pathlength of 1 cm and the spectra were recorded at an excitation and emission wavelength of 280 nm and 340 nm respectively with a slit width of 5 nm for both excitation and emission. The concentrations used for the measurement were 5 µM for ALP, 1 and 10 mM for metal ions (Zn^{2+}, Mg^{2+}, Ca^{2+} & Na^+) and 100 mM for sugars (Fructose, Glucose, Sucrose). The spectra were recorded over a range of 300 nm to 500 nm.

1.4 Measurement of anisotropy of Alkaline phosphatase:

Steady state anisotropy measurements of alkaline phosphatase (ALP) were performed on an LS 55 luminescence spectrometer from Perkin Elmer at an excitation and emission wavelength of 280nm and 340 nm respectively with a band pass of 5 nm for excitation and 6 nm for emission. The concentration used of the measurement were 5 µM for ALP, 1mM for metal ions (Zn^{2+}, Mg^{2+}, Ca^{2+} & Na^+) and 100 mM for sugars (Fructose, Glucose, Sucrose).

## 1.5 Measurement of Alkaline phosphatase catalytic activity:

The catalytic activity measurements of enzyme ALP were performed spectrophotometrically using p-nitrophenyl phosphate (PNPP) as substrate in buffer. AP catalytic activity was also determined in presence of all sugars (Fructose, Glucose, Sucrose & Maltose) and metal ions (Zn, Mg, Ca & Na) separately and in presence of both (metal ions & sugars) in Buffer. For activity, 100 nM AP along with fixed concentration of substrate i.e., 250 µM with 100 mM of sugars and 1 mM ions were used for recording enzyme's catalytic activity in 10 mM pH: 7 HEPES buffer.

1.6 Microfluidics Study:

For microfluidics studies, a syringe pump from World Precision Instruments and microfluidic channels from Venadelta made of acrylic plastic material were used. For 2-inlet channel, using a

syringe pump, 5 µM of ALP (5% labelled + 95% unlabelled) in 10mM HEPES Buffer (pH=7) was injected from the top inlet while 100mM Sugars, 1mM Ions, 100mM Sugar-1mM Ions in 10mM HEPES buffer(pH=7) were injected from the bottom inlet. Similarly, in case of 3-inlet channel, through middle channel, FITC-ALP was injected and from the top and bottom channel, sugar and cation solution, respectively were injected. Images were acquired at both inlet and outlet at similar gain, brightness and contrast for each set of experiments. The fluorescence intensity profile was analysed via ImageJ software.

2. Circular Dichroism Studies
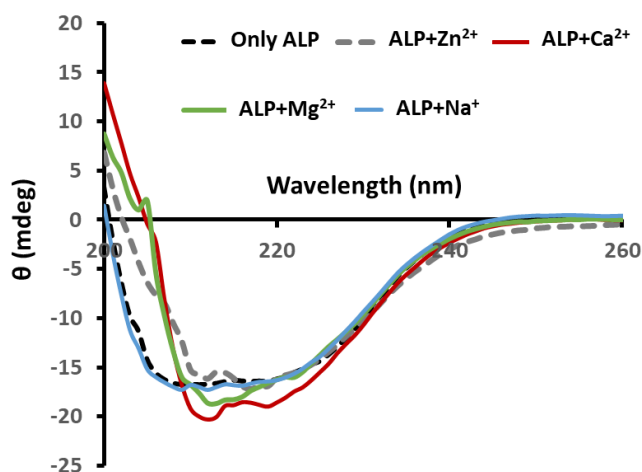
Fig. S1: Circular Dichroism (CD) spectra of only enzyme (ALP) along with different metal in aqueous buffer (HEPES, pH = 7). Experimental condition: [ALP] = 2 µM, [Sugars] = 100 mM, [Metal ions]: 1 mM, CD cuvette pathlength = 1 mm, HEPES buffer (10 mM, pH = 7), T=25 °C.
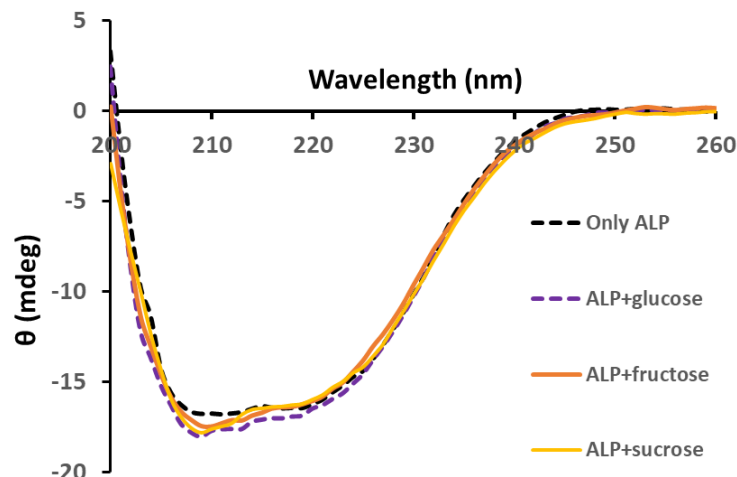
Fig. S2: Circular Dichroism (CD) spectra of only enzyme (ALP) along with different metal in aqueous buffer (HEPES, pH = 7). Experimental condition: [ALP] = 2 µM, [Sugars] = 100 mM, [Metal ions]: 1 mM, CD cuvette pathlength = 1 mm, HEPES buffer (10 mM, pH = 7), T=25 °C.
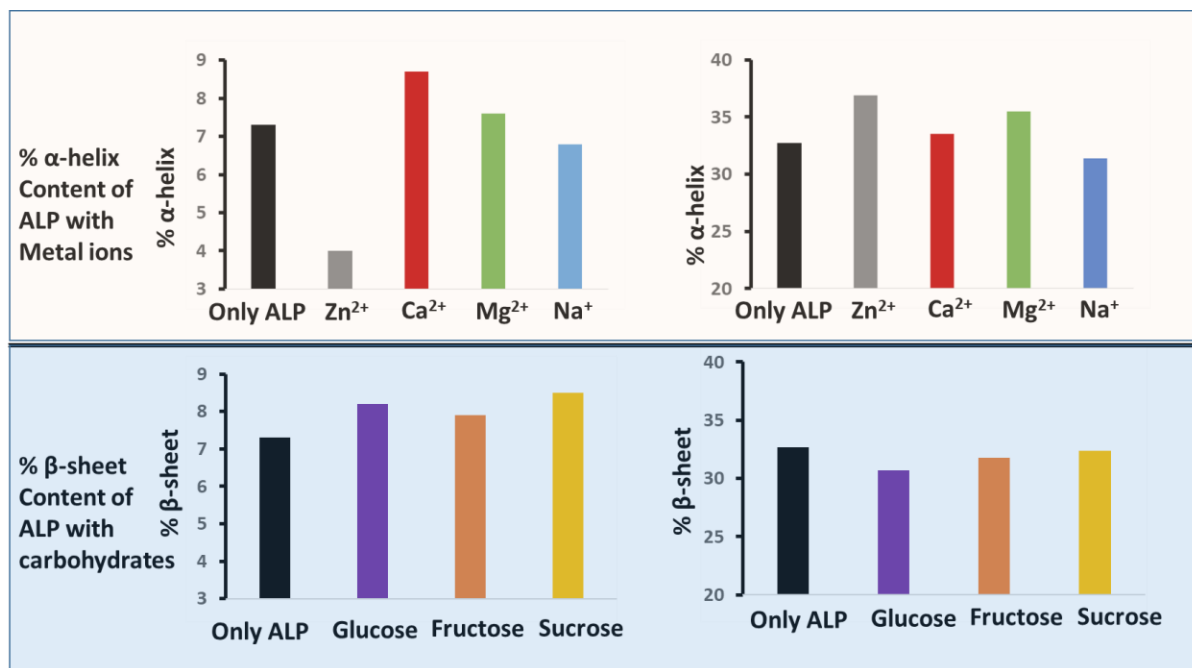

Fig. S3. Percentage content of the α helix and β sheet of alkaline phosphatase in absence and presence of metal ions and carbohydrates. The calculation was performed by analyzing the above-mentioned CD spectra as reported in the literature.[S2] The helical content of native alkaline phosphatase was corroborated with earlier literature reports.[S3]

Interestingly, here for carbohydrates no loss of helical structure was observed, rather in each case, enhancement in α-helix content was observed, suggesting further stability of the enzyme

as reported in previous literature.[S4] However, for Zn^{2+}, noticeable decrease in α-helix content and increase in β-sheet content was observed, indicating binding of the ion and corresponding change in the secondary structure of the enzyme. For Na^+, least alteration in helical content was observed. Interestingly, for Ca^{2+} and Mg^{2+}, increase in helical content was observed, indicating binding and retention of enzyme stability. These secondary structural analyses, also corroborating with tertiary structure alteration study as shown in Fig. 2b and c, where only in presence of Zn^{2+}, significant loss of tertiary structure of the enzyme was observed.

3. Kinetics Measurements:
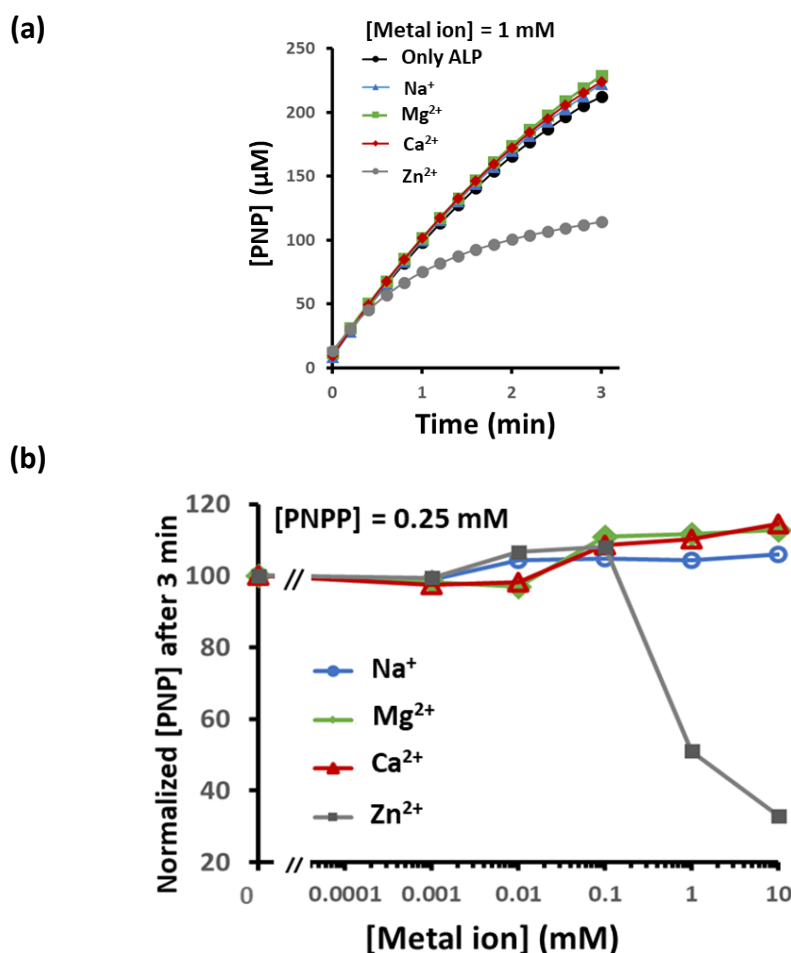
Fig. S4. Normalized yield of the hydrolysed PNP as a function of different metal ion concentration. (b) Hydrolysis of p-nitrophenylphosphate (PNPP) by ALP in presence of different metal ions (1 mM) as a function of time monitored by following the absorbance of the hydrolysed product p-nitrophenol (PNP) (extinction coeff= 7000 $M^{-1}cm^{-1}$ was used to calculate concentration of the liberated PNP). [PNPP] = 250 µM, [ALP] = 0.1 µM, [HEPES] = 10 mM, pH = 7.
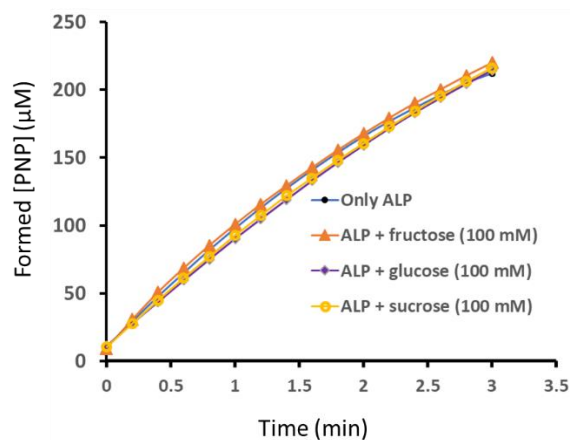
**Fig. S5:** Representative plot of initial rate (Vi) kinetics of ALP with different sugars. Experimental conditions: [PNPP]= 250 µM, [ALP]: 100 nM, [Carbohydrates]: 100 mM, HEPES buffer (10 mM, pH = 7), T=25 °C.
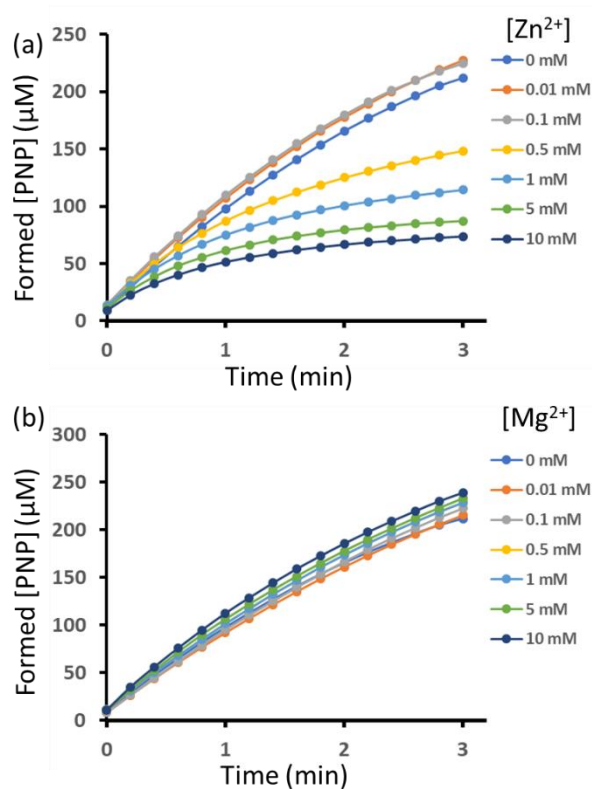
Fig. S6: Representative plot of initial rate (Vi) kinetics of ALP with different concentration of Zn^{2+} and Mg^{2+}. Experimental conditions: [PNPP]= 250 µM, [ALP]: 100nM, [metal ions]: 0-10 mM, HEPES buffer (10 mM, pH = 7), T=25 °C.

4. Dynamic Light Scattering Study:
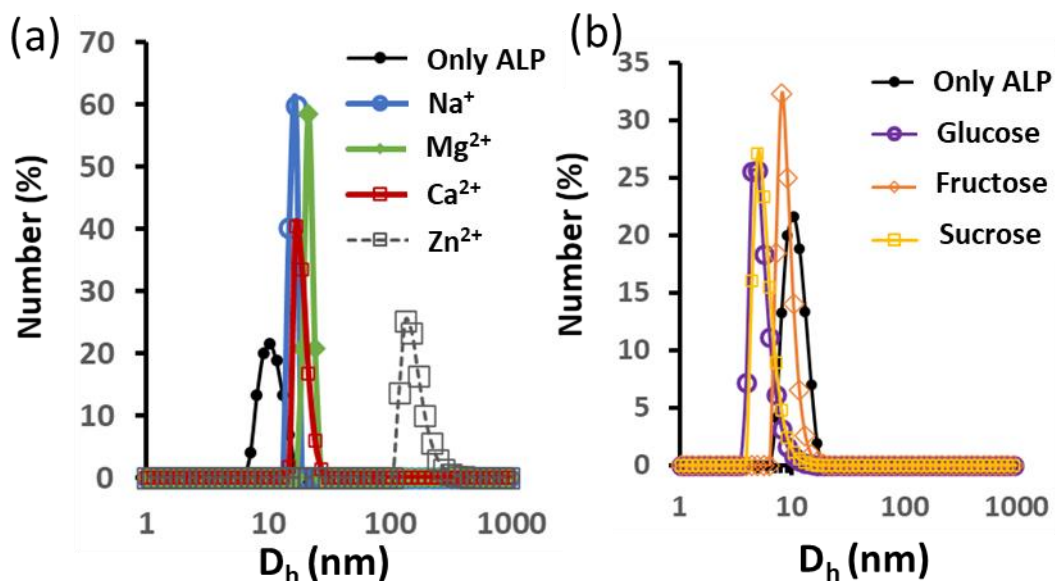
Fig. S7. Dynamic light scattering profile of ALP in (f) presence of metal ion (1 mM) and (g) carbohydrates (100 mM). [ALP] = 5 μM, [Carbohydrates]: 100 mM, [Metal ion] = 1mM, HEPES buffer (10 mM, pH = 7), T=25 °C.

In presence of Zn^{2+} (1 mM), hydrodynamic diameter (D_h) of native ALP gets enhanced by almost one order of magnitude, clearly suggesting aggregation of ALP at 1 mM Zn^{2+}. However, for Mg^{2+} and Ca^{2+}, no such striking change in dimension was observed. Interestingly, in presence of carbohydrates (100 mM), the D_h of ALP slightly decreased, suggesting further compactness of the enzyme.

5. Anisotropy measurements
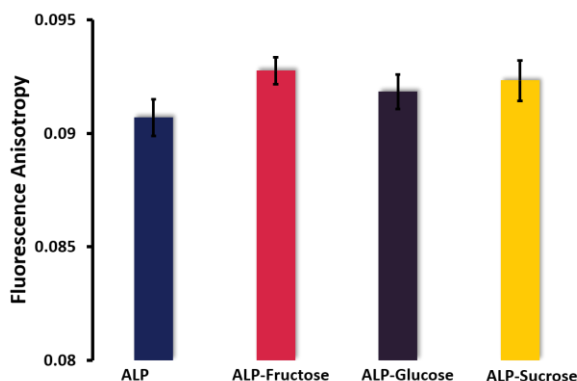
Fig. S8. Representative bar graph showing Anisotropy values of different system containing enzyme. Experimental condition: [ALP]: 2 µM, [Sugars]: 100 mM, HEPES Buffer (10 mM, pH = 7), T=25 °C.

We also checked the fluorescence anisotropy of the native ALP by observing its tryptophan fluorescence. It is to be noted here that fluorescence anisotropy is a measure of rota-tional mobility of the enzyme which increase in confined environment (Ref. 11 of the main manuscript). Anisotropy data clearly suggest aggregation and restricted mobility of ALP takes place in presence of 1 mM of Zn^{2+} among others.

In presence of Zn^{2+} (10 mM) the steady state fluorescence anisotropy value increased by ~20 % suggesting aggregation of the ALP (Fig. 2d in the main manuscript). The enhancement is only by 5% and 4% in case of Mg^{2+} and Ca^{2+}. In fact, even at 1 mM of Zn^{2+}, the anisotropy value of native ALP enhanced by 5%, whereas with other ions at 1 mM concentration or with carbohydrates no significant change in anisotropy value were observed (Fig. S5).

6. Viscosity measurements:

Table S1: Calculated viscosities of sugar solutions with respect to water.

Sample	Viscosity (dyne-s /cm²)
Water only	0.0089 as reference
100 mM Glucose	0.009
100 mM Fructose	0.0089
100 mM Sucrose	0.0090
200 mM sucrose	0.0104
500 mM sucrose	0.0122
1000 mM sucrose	0.0283

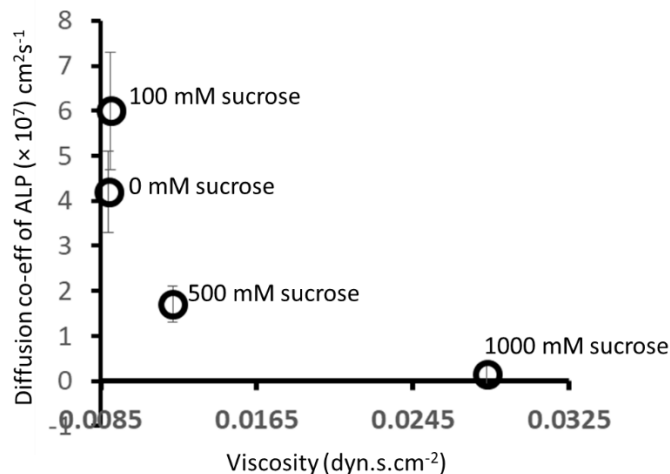## 7. Diffusion co-efficient and Zeta Potential measurements:
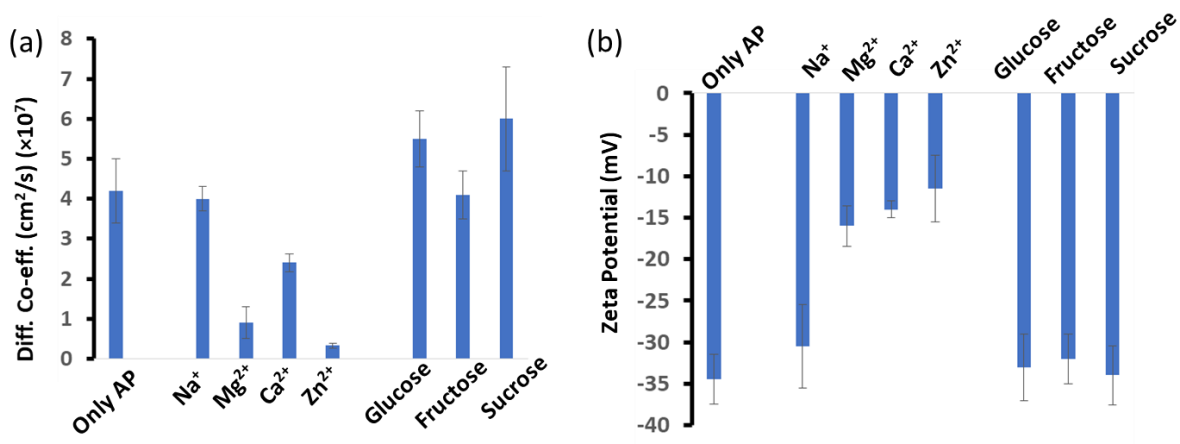
Fig. S9. (a) Diffusion co-efficient and (b) zeta potential values of ALP (5 µM) in presence of metal ions (1 mM) and carbohydrates (100 mM). [HEPES] = 5 mM, pH = 7.

This selective aggregation of ALP in presence of Zn^{2+} is also clear upon analyzing the diffusion coefficient (DC) data (Fig. S9a). The diffusion co-efficient of only ALP was found ~4 × 10^{-7} cm²/s, similar to previously reported literature with other protein and enzymes (Ref. 12 of the main manuscript). Herein also, in presence of carbohydrates no such change in DC of native ALP was

observed, rather slight enhancement in DC value was observed indicating decreased size of native ALP.

It is worthy to mention we limited carbohydrate concentration up to 100 mM, in all our study to avoid any effect which comes from viscosity (Table S1, Fig. S10, ESI).


Fig. S10. Diffusion co-efficient of ALP as a function of viscosity of sucrose solution.
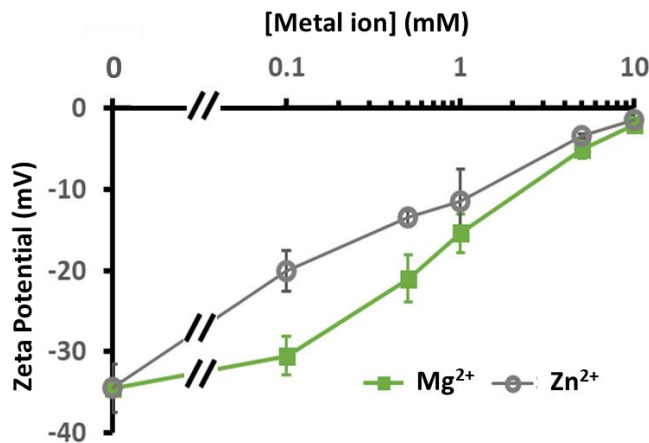
Fig. S11. Zeta potential values of ALP (5 µM) in presence of different concentration of Mg^{2+} and Zn^{2+} (1 mM). [HEPES] = 5 mM, pH = 7.

This experiment suggest binding of ALP with both Mg^{2+} and Zn^{2+}, however, extent of binding is much more in case of Zn^{2+}. Interestingly, native activity of the enzyme did not decrease in presence of even 10 mM Mg^{2+}, unlike Zn^{2+} although the zeta potential became close to zero (please see Fig. S6). This also indicates Zn^{2+}-binding induced aggregation of ALP and alteration of native helical structure of ALP which is detrimental for the enzyme activity.
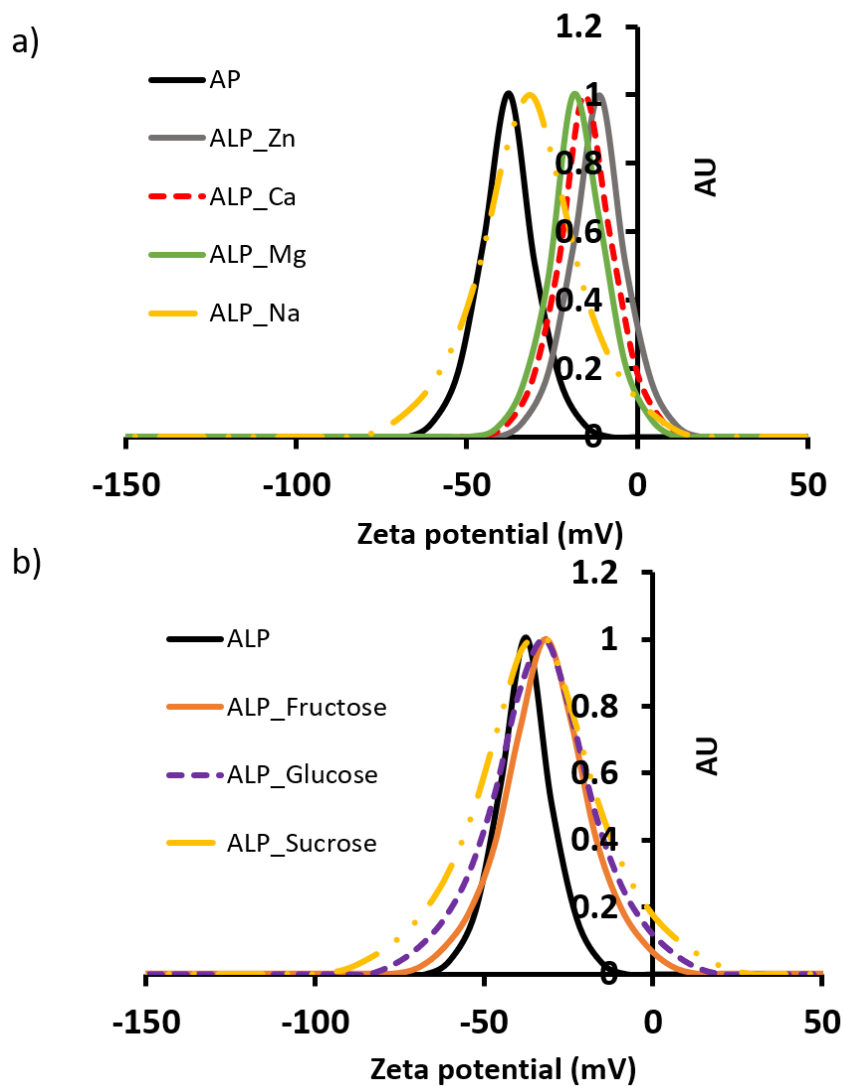
Fig. S12. Characteristic plots of enzyme with a) metal ions and b) sugars respectively showing zeta potential values of each system. Experimental condition: [ALP]: 5 μM, [Metal Ions]: 1 mM, [Sugars]: 100 mM, HEPES Buffer (10 mM, pH = 7), T=25 °C.

Table S2: Zeta potential values of Alkaline phosphatase in presence of metal ions and carbohydrates. Experimental conditions: [ALP]: 5μM, [Metal ions]: 1 mM, [Carbohydrates]: 100 mM, HEPES buffer (10 mM, pH = 7), T=25 °C.

Carbohydrate	Metal ion	Zeta potential (mV)
-	-	-33.5 ± 3 mV
Glucose	-	-33.5 ± 0.8 mV
	Na^+	-30.1 ± 0.9
	Mg^{2+}	-20.5 ± 0.4
	Ca^{2+}	-12.7 ± 0.6
	Zn^{2+}	-12.1 ± 0.3
Fructose	-	-32.2 ± 0.3
	Na^+	-29.0 ± 0.5
	Mg^{2+}	-22.1 ± 0.3
	Ca^{2+}	-11.9 ± 0.4
	Zn^{2+}	-11.6 ± 0.4
Sucrose	-	-33 ± 0.2
	Na^+	-27.3 ± 0.6
	Mg^{2+}	-15.3 ± 0.4
	Ca^{2+}	-11.2 ± 0.5
	Zn^{2+}	-11.5 ± 0.2

8. Hydration energies:
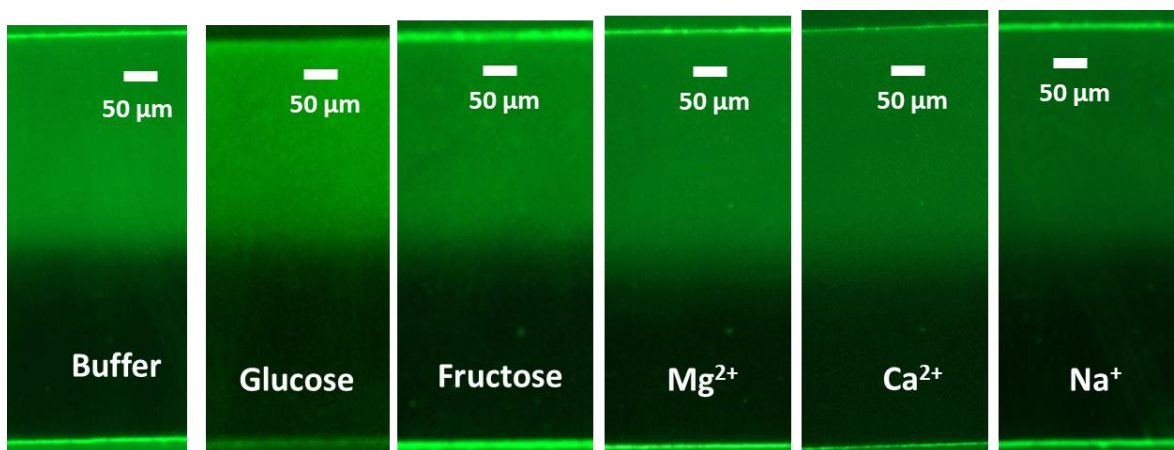
Table S3: Hydration energies of metal salt solutions and sugar solutions[S5,S6]

| System	ΔH_{hyd}/ KJmol^{-1}
Zn^{2+}	-1966
Mg^{2+}	-1953
Ca^{2+}	-1615
Na^+	-424
Glucose	-375
Sucrose	-600

9. Microfluidics Images
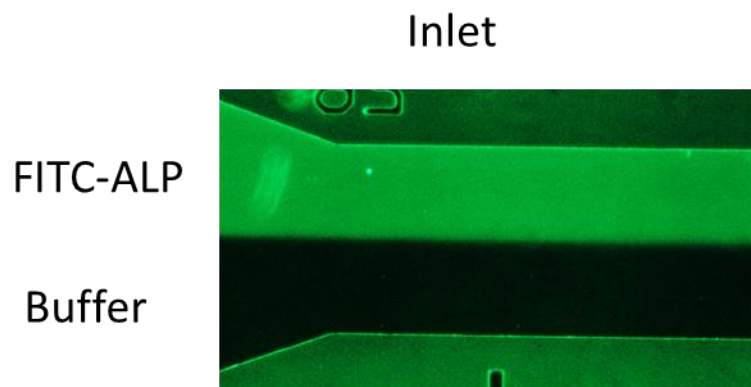
Fig. S13. Typical Fluorescence microscopic images of 2-inlet and 1-outlet of the microfluidics channel with a flow rate of 0.16 ml/hr from each inlet, controlled by using a syringe pump.

Fig. S14: Representative fluorescence microscopic images near outlet (1.6 cm apart) of microfluidics experiment in 2-inlet channel where **Top inlet:** ALP in 10mM HEPES Buffer (pH=7) and **bottom inlet:** Buffer, glucose, fructose, Mg^{2+}, Ca^{2+} and Na^+ in buffer. White dotted line is a guide to show the drift from center. Experimental conditions: [ALP]: 5 µM, [Metal ions]: 1 mM, HEPES buffer (10 mM, pH = 7), T = 25 °C. In each cases nitrate salt has been used. Schematic of the microfluidic set up has been provided in Fig. 3a of the main manuscript.
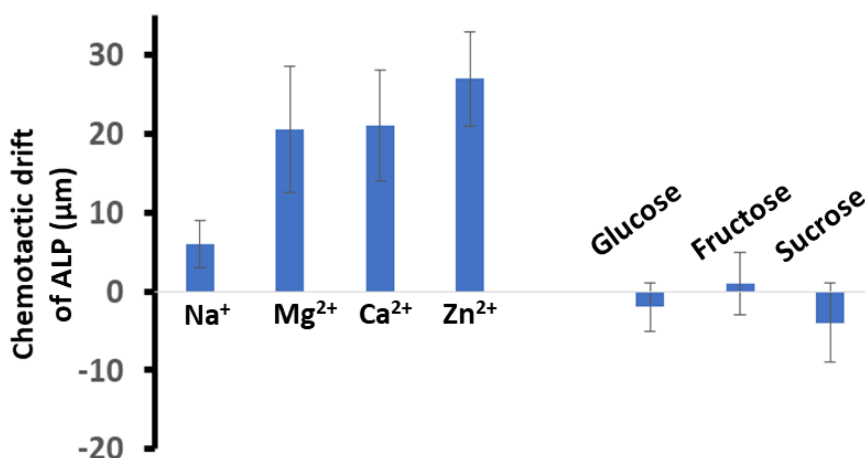
Fig. S15. Chemotactic drift of ALP in response to gradient of metal ion and carbohydrates. The drift was calculated at the half height of fluorescence intensity as indicated by dotted black arrow in the Fig. 3c of the main manuscript. Right and left shift from the native ALP in response to only buffer was denoted as +ve drift and –ve drift, respectively. The error bar is the standard deviation of three independent experiments in each cases.

ALP drift analysis under static condition:

35 µl of sugar or salt solution was added over glass slide and then cover slide was placed above the solution such that the solution became uniformly distributed under the cover slip. Then after from one side 1 µl of FITC-ALP drop was added, the drop started diffusing and the image was captured using the microscope immediately in 30 seconds. For each sample, experiments were performed in triplicate. All of the sample's images were analyzed using ImageJ software.
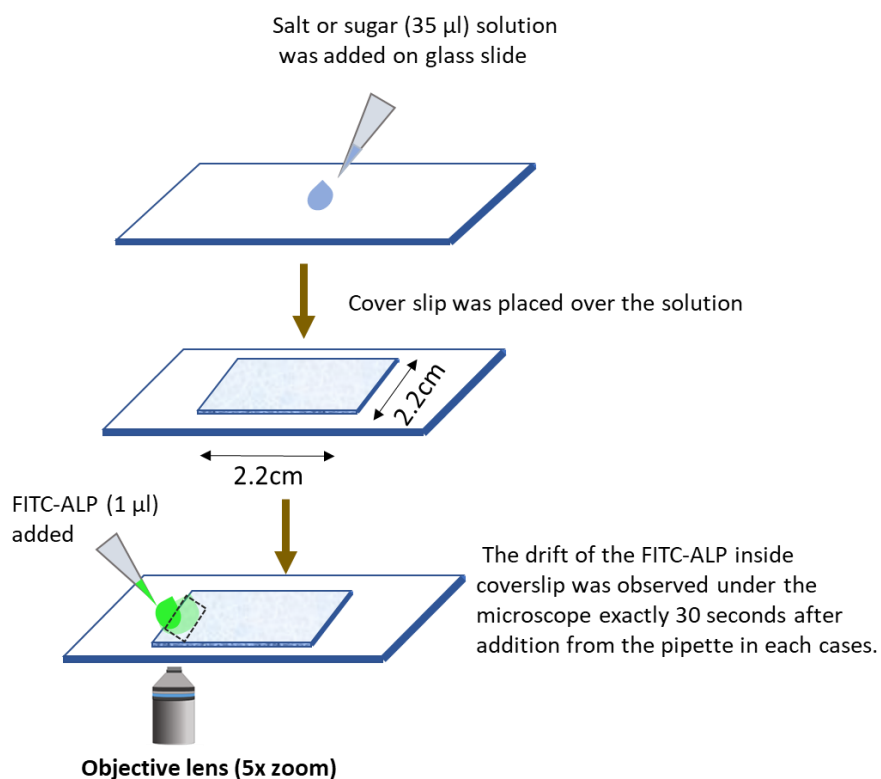

Fig. S16. Schematic representation of experimental set up for studying drift of FITC-ALP through sugar or salt solution present under cover slip.
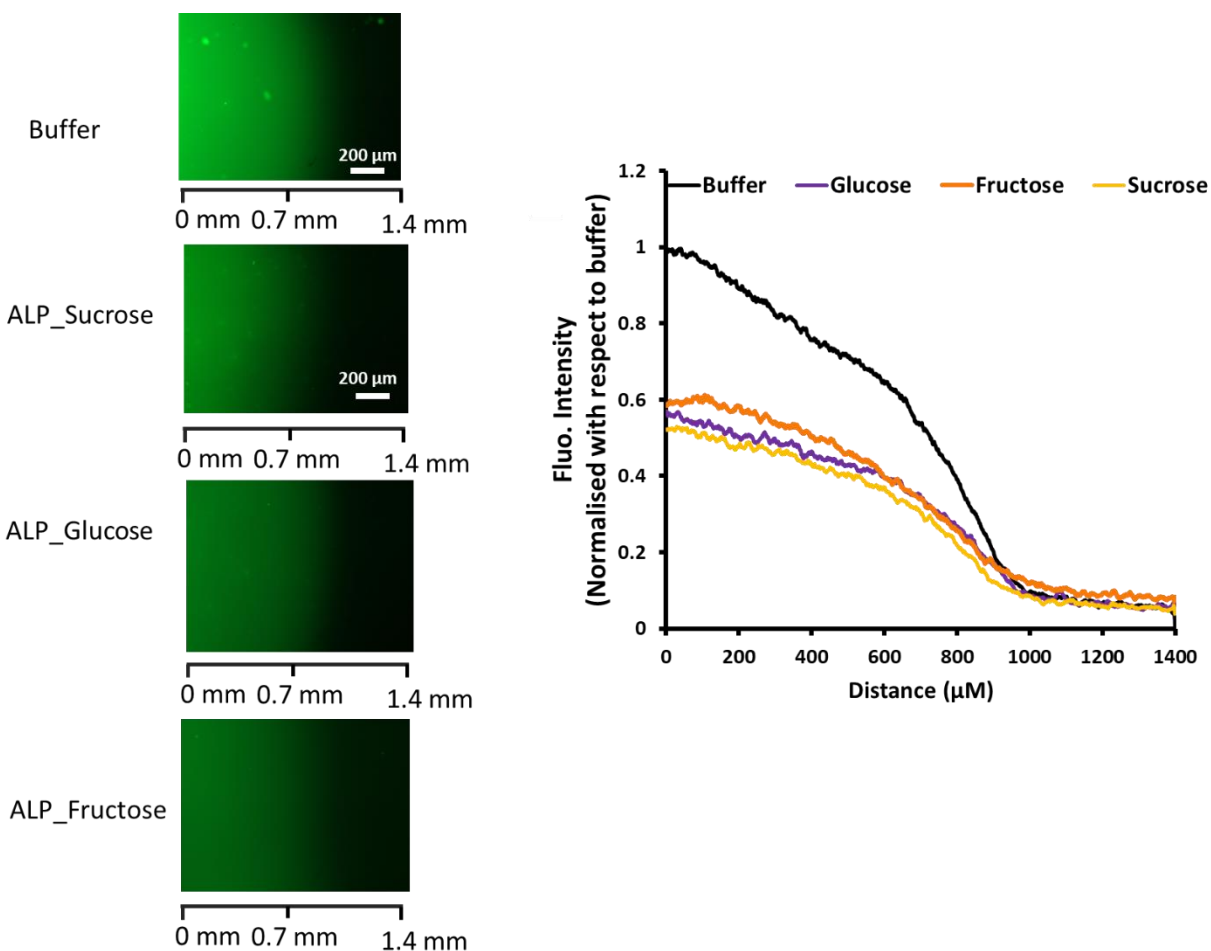
Fig. S17. Microscopic images taken 30 sec after addition of FITC-ALP (1 µl) from 5 µM stock in HEPES buffer (5 mM, pH 7) at the edge of the cover slip as shown in Fig. S16. The images were taken from just inside the edge of the coverslip to capture the diffusion of the enzyme inside coverslip. Inside of the coverslips contains either only buffer, sucrose, fructose or glucose solution (100 mM) dissolved in buffer. X-axis of each images were 1.4 mm. In the right panel, fluorescence intensity profile based on distance along the x-axis was plotted. Herein, we have done 3 sets of experiments in each cases. One representative set of images and average intensity plot was given. The diffusion of enzyme inside cover slip is clearly less than only buffer when carbohydrates were placed inside the cover slip. This experiment also corroborated with our 2-inlet microfluidic experiment where slightly negative drift was observed (Fig. S15).
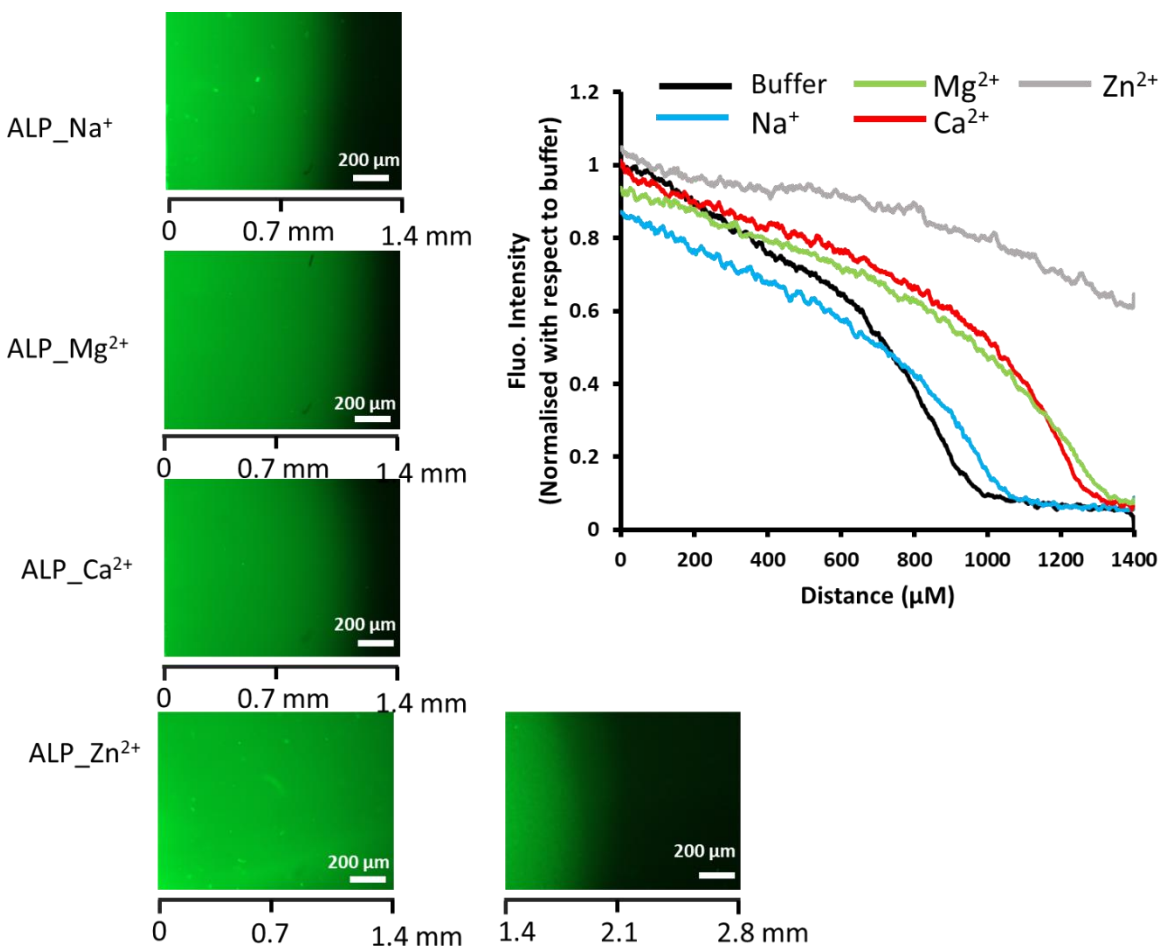
Fig. S18. Microscopic images taken 30 sec after addition of FITC-ALP (1 μl, from 5 μM stock) at the edge of the cover slip as shown in Fig. S16. The images were taken just inside the edge of the coverslip to capture the diffusion of the enzyme inside coverslip from outside. Inside of the coverslips contains either Na^+, Mg^{2+}, Ca^{2+} or Zn^{2+} solution (1 mM) with nitrate as counter anion. X-axis of each images were 1.4 mm. In the right panel, fluorescence intensity profile based on distance along the x-axis was plotted. Herein, we have done 3 sets of experiments in each cases. One representative set of images and average intensity plot was given. The diffusion of enzyme inside cover slip is clearly more than only buffer when divalent ions (Ca^{2+}, Mg^{2+} and Zn^{2+}) were placed inside the cover slip. Here also drift was negligible when Na^+ was kept inside the coverslip and for Ca^{2+} and Mg^{2+}, similar trend was observed. This experiment also corroborated with our 2-inlet microfluidic experiment where positive drift for metal ion was observed (Fig. S15). Interestingly, in case of Zn^{2+}, the observed drift was very high and the lens need to move to another frame (1.4-2.8 mm zone) to capture the total drift of ALP.
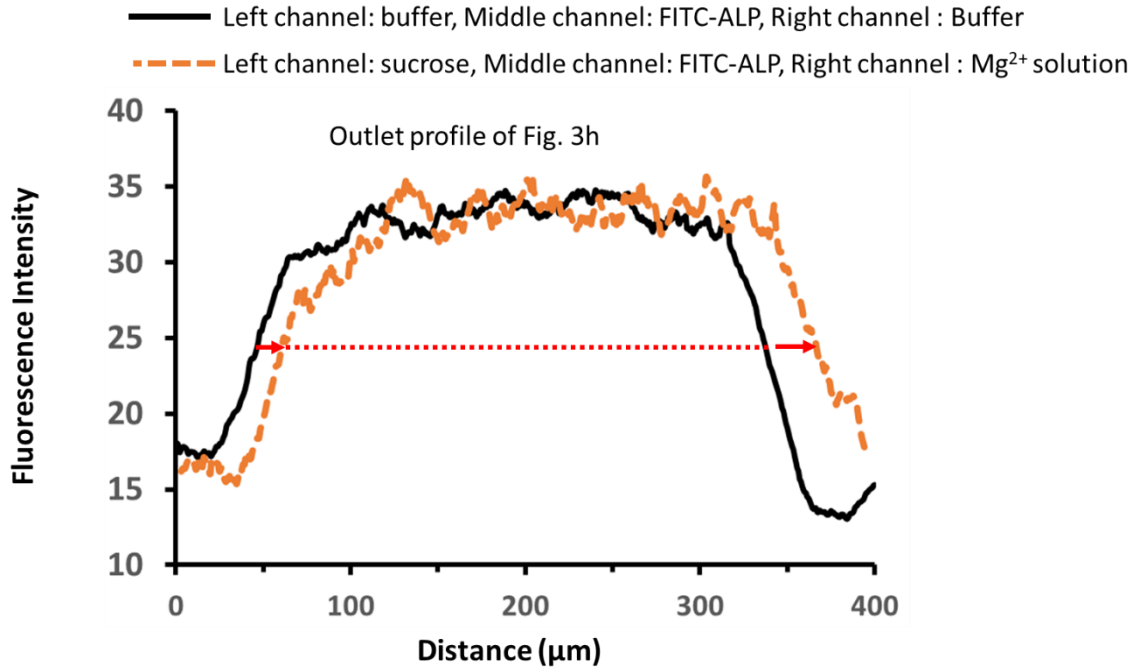
Fig. S19. Fluorescence intensity profile FITC-ALP in 3-inlet channel described in Fig. 3g and h of the main manuscript was shown. Red arrow indicated negative drift away from sucrose gradient and positive drift towards Mg^{2+} ion.

10. Rationalization of Phoretic Drift:

The generalized equation for calculation of diffusiophoretic velocity is the following eqn S1:

$$U_{dp} = \frac{\varepsilon kT}{\eta Ze} \left\{ \beta \zeta - \frac{2kT}{Ze} \ln \left[1 - tanh^2 \left(\frac{Ze\zeta}{4kT} \right) \right] \right\} \frac{\nabla C}{C} \qquad \text{............ (S1)}$$

This is a generalized equation combining both electrophoresis and chemiphoresis part, where first part is the electrophoretic component.[S6]

Here, U$_{dp}$ = diffusiophoretic velocity; ε = permittivity of medium (6.9 × 10^{-10} Fs^{-1});

k_B = 1.38 × 10^{-23} J K^{-1}, T = 298 K, e = 1.6 × 10^{-19} C and μ = 10^{-3} Pa.s, Z is the charge of the ions involved.

Now, considering enzyme in a gradient of salt with different β-value, the diffusiophoretic velocity will mainly depend on βζ-term.

Now, $\beta = \frac{D_+ - D_-}{z_+ D_+ - z_- D_-}$ and ζ is the zeta potential of the particle (here enzyme).[S7] D$_+$ and D$_-$ are the diffusion coefficient of cation and anion, respectively.

Table S4. Electrophoretic velocity of ALP in presence of different salt gradient considering $\nabla C/C$ = 1 mm^{-1} from eqn S1. Diffusion co-efficient of NO_3^- = 1.9 × 10^{-9} m^{2}s^{-1}, D_{Na+} = 1.33 × 10^{-9} m^{2}s^{-1}; $D_{Mg}{}^{2+}$ = 0.705 × 10^{-9} m^{2}s^{-1}; $D_{Ca}{}^{2+}$ = 0.793 × 10^{-9} m^{2}s^{-1}, $D_{Zn}{}^{2+}$ = 0.715 × 10^{-9} m^{2}s^{-1}

Salt	Concentration of salt (mM)	β- value	ζ- of ALP in presence of salt (mV)	Electrophoretic velocity of ALP (µm/s)
NaNO₃	1	-0.17	-30.5	46.8
Ca(NO₃)₂	1	-0.32	-14	38.6
Zn(NO₃)₂	1	-0.35	-11.5	35.6
Mg(NO₃)₂	1	-0.36	-16	50.2
Zn(NO₃)₂	10	-0.35	-1	3.1
Mg(NO₃)₂	10	-0.36	-3.5	10.9

We reasoned this opposite directional behaviour of ALP chemotaxis with carbohydrates and metal ions using Hofmeister phenomenon where hydration energy (ΔH_{hyd}) of the ions or other solutes played crucial role. Carbohydrates molecules are rich in hydroxyl groups and thus well-hydrated in aqueous solution. These types of molecules do not tend to bind with hydrophobic inner core of the enzyme or proteins. In fact, these molecules have a tendency – (i) to capture water molecules from the hydration layer of the enzyme and (ii) get repelled by the hydrophobic part of the enzyme. In our case, the ΔH_{hyd} of glucose and sucrose are -375 and -600 KJ/mol, respectively.[S5] In both the cases, we did not observe any aggregation due to loss of hydration layer from the enzyme vicinity, unlike carbonate anion (ΔH_{hyd} = - 1389 KJ/mol). In fact, in presence of 100 mM carbonate anion (one of the strongest kosmotropic anion) we also observed –ve chemotactic drift of ALP (-18 µm) (which is even higher than sucrose) (Fig. S20, ESI). Therefore, the hydration energy driven interaction is mainly responsible for –ve chemotactic drift (Ref. 5 of the main manuscript). Now, in our case, divalent metal ions have 3-5 -fold higher ΔH_{hyd} than carbohydrates, but still in these cases we observed +ve chemotactic drift. Divalent metal ions have the co-ordinating ability with the core amino acid residue of the enzyme molecules which also reflects in their ability to decrease the native zeta potential of the enzyme. Herein, we correlated the chemotactic drift by their binding based on zeta potential decreasing ability and hydration energy (Table S3, SI). We assumed negative hydration energy as the repulsive factor leading to –ve chemotaxis, whereas any change in zeta potential corresponds attractive factor in

terms of positive change in hydration energy. Thus, in each case we calculated effective ΔH_{hyd} (EHH) as following equation:

EHH = $[-(\Delta\zeta \times (\Delta H_{hyd}))+(\zeta_{final} \times \Delta H_{hyd})]/\zeta_{native\ ALP}$ ... (S2)

Here, $\Delta\zeta$ and ΔH_{hyd} are the decrease in ζ of native ALP upon adding ions or carbohydrates and hydration energy of the ions or carbohydrates and $[-(\Delta\zeta \times (\Delta H_{hyd}))]$ this term contributed as attractive factor. ζ_{final} stands for final ζ of the ALP after binding and ($\zeta_{final} \times \Delta H_{hyd}$) contributed overall repulsive factor and $\zeta_{native\ ALP}$ is the ζ of the native ALP (-34.5 mV). Now upon plotting EHH against chemotactic drift, we obtained a reasonably good correlation which accounts both ζ-potential and ΔH_{hyd} proportionately and explains well the reason for their chemotactic behaviour (Fig. S21). Here positive EHH corresponds to higher positive drift, whereas, negative EHH corresponds to low positive or negative drift. This positive EHH can also be assumed as additional osmotic or entropy related contribution towards their phoretic behaviour (also see Ref. 16 of the main manuscript). Thus, for Zn^{2+} although the electrophoretic mobility will be lesser, but due to much higher EHH (most decrease in native zeta value of ALP), osmotic pressure difference was higher, resulting net higher phoretic drift.

We also checked the ALP migration at higher Zn^{2+} and Mg^{2+} (10 mM), as here the zeta potential of ALP becomes close to zero (-1 and -3.5 mV for Zn^{2+} and Mg^{2+}, respectively) and thus electrophoretic mobility should be decreased drastically (Table S4, ESI). In fact, we also observed the overall drift of the ALP decreased while performing the experiment in a static platform as described in Fig. S22. Although in this case, considerable positive drift up the ion gradient was observed. Therefore, we can assume in this case, the contribution towards phoresis comes mostly from binding induced osmotic pressure increase as theoretically electrokinetic-driven effect will be negligible.

Notably, here we did not consider change in DC value of native ALP, for the consideration of chemotactic drift. Experimentally, we observed lowest DC for Zn^{2+}-containing ALP which should result –ve chemotactic drift.[S9] In contrary, here we observed maximum chemotactic drift for Zn^{2+} which allows us to neglect the DC factor.
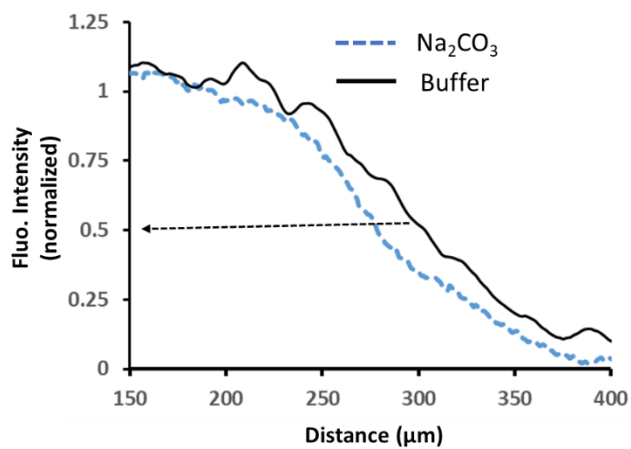
Fig. S20. Representative normalized fluorescence intensity profile FITC-ALP in gradient of Na_2CO_3 (100 mM). Please see Fig. 3a for experimental set up.
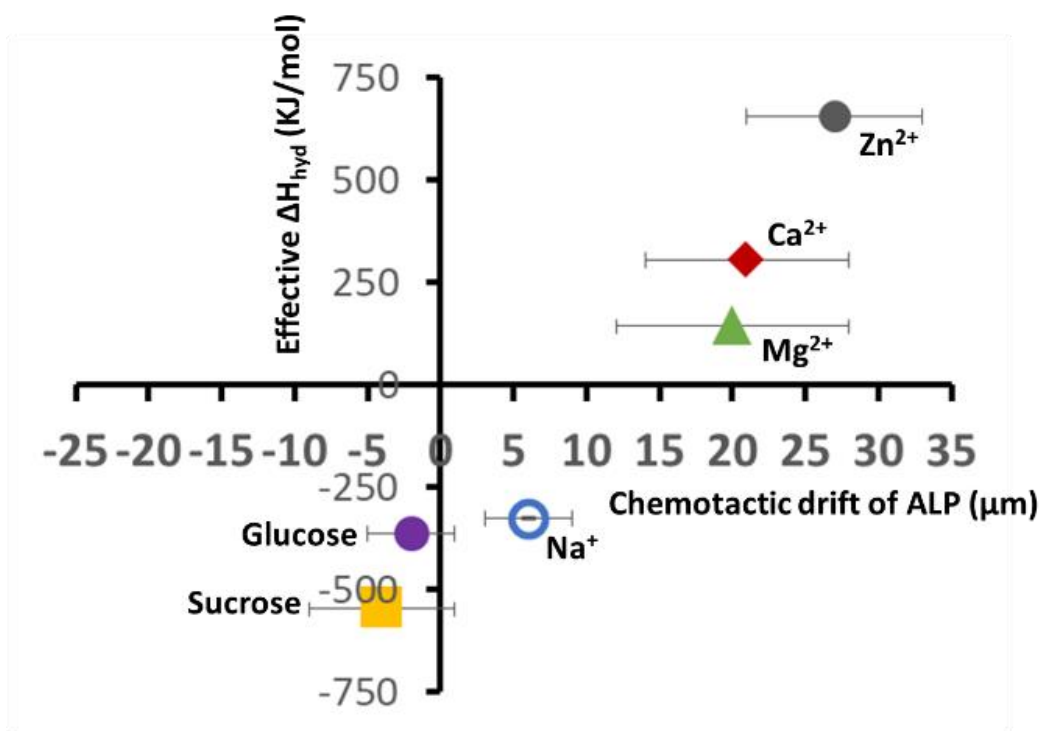
Fig. S21. Plot of Effective ΔH_{hyd} as a function of chemotactic drift of ALP in our experimental condition. Please see equation S2 for the calculation of EHH.
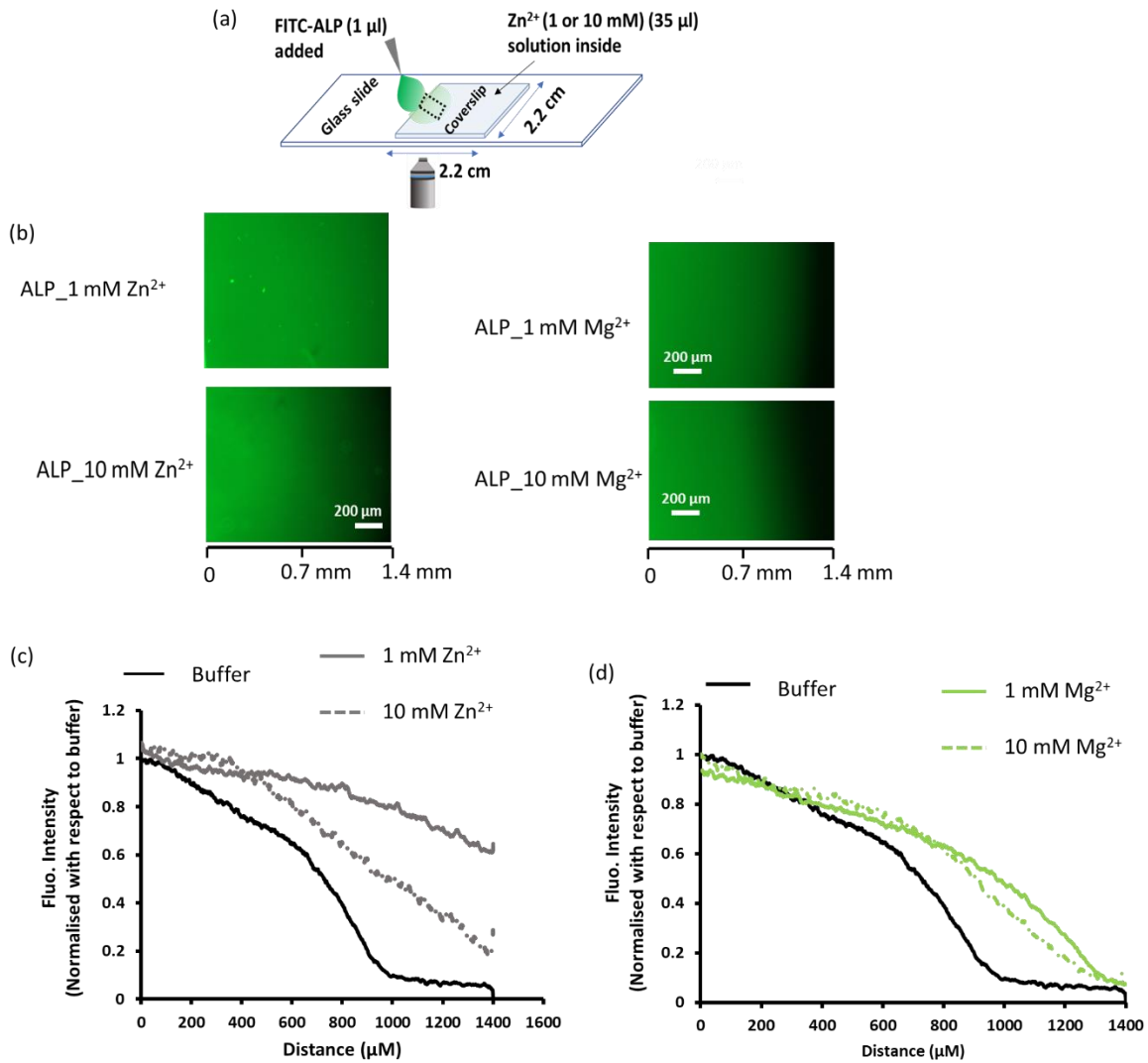
Fig. S22. (a) Schematic representation and (b) microscopic images of the penetration of fluorescent ALP when Mg^{2+} or Zn^{2+} (1 or 10 mM) was kept under the coverslip. (c-d) Fluorescence intensity profile based on distance along the x-axis was plotted. This showed at higher concentration of Zn^{2+} or Mg^{2+}, the phoretic drift of ALP from low to high concentration of metal ion decreased. It overall indicated dominant role of osmotic pressure, rather than electrophoretic driven flow (As in presence of 10 mM Zn^{2+} and Mg^{2+}, the ζ-value of ALP becomes close to zero (only -1 and -3.5 mV for Zn^{2+} and Mg^{2+}, respectively).
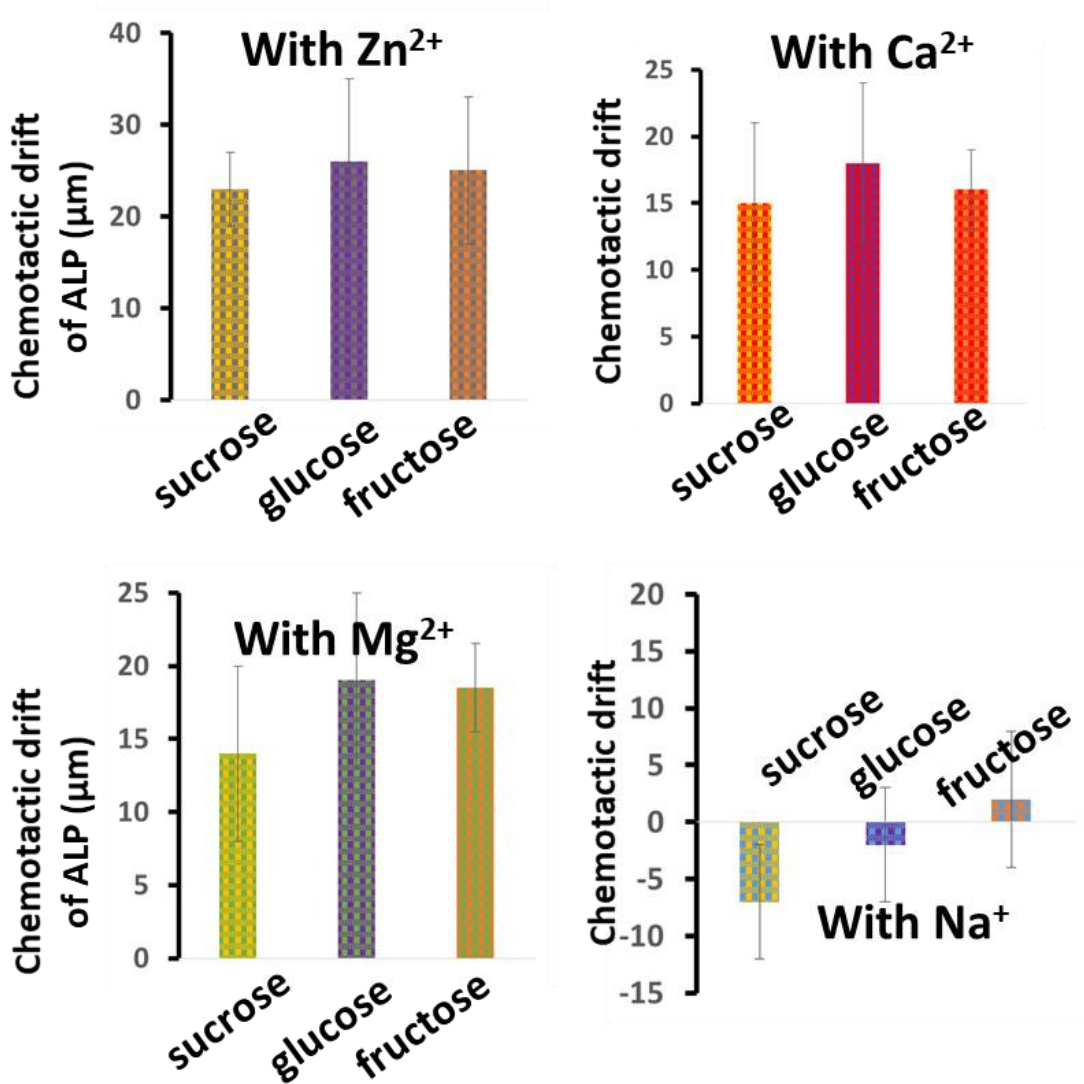
Fig. S23. Chemotactic drift of ALP when carbohydrates (100 mM) were mixed with Zn^{2+}, Ca^{2+}, Mg^{2+} and Na^+ when passed through a 2-inlet microfluidic channel as described in Fig. 3a and 3c in the main manuscript. [Metal ion] = 1 mM.

10. References:

S1. S. Rani, B. Dasgupta, G. K. Bhati, K. Tomar, S. Rakshit and S. Maiti. *ChemBioChem* 2020, **22**, 1285-1291.

S2. A. Micsonai, F. Wien, E. Bulyáki, J. Kun, E. Moussong, Y. -H. Lee, Y. Goto, M. Réfrégiers and J. Kardos. *Nucleic Acids Res.* 2018, **46**, W315– W322.

S3. M. L. Applebury and J. E. Coleman, *J. Biol. Chem.* 1969, **244**, 308-318.

S4. S. Sekiguchi, Y. Hashida, K. Yasukawa and K. Inouye, *Biosci. Biotechnol. Biochem.* 2012, **76**, 95-100.

S5. J. Teychené, H. Roux-de Balmann, L. Maron and S. Galier. *Food Chem.* 2020, **327**, 127054.

S6. A. A. Merdaw, A. O. Sharif and G. A. W. Derwish, *Chem. Eng. J.* 2011, **168**, 229–240.

S7. D. Velegol, A. Garg, R. Guha, A. Kar and M. Kumar, *Soft matter*, 2016, **12**, 4686-4703.

S8. A. Persat and J. G. Santiago, *Curr. Opin. Colloid Interface Sci.* 2016, **24**, 52.

S9. F. Mohajerani, X. Zhao, A. Somasundar, D. Velegol and A. Sen, *Biochemistry*, 2018, **57**, 6256–6263.